Metallomics

Accepted Manuscript

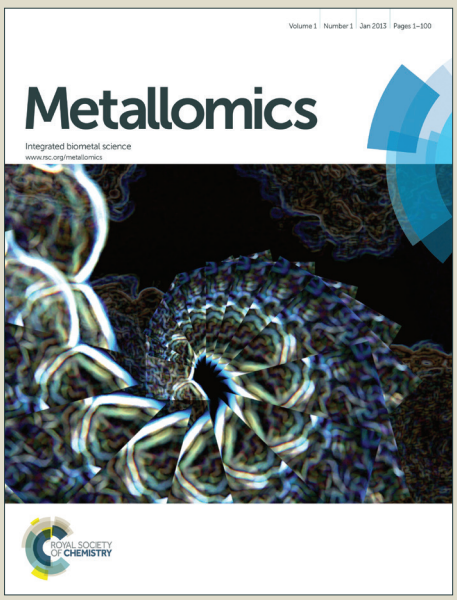

ROYAL SOCIETY OF CHEMISTRY

www.rsc.org/metallomics

A novel branched TAT_{47-57} peptide for selective Ni^{2+} introduction into the human fibrosarcoma cell nucleus

Łukasz Szyrwiel[a,b,*], Mari Shimura[b,c,d,*], Junko Shirataki[e], Satoshi Matsuyama[d,f], Akihiro Matsunaga[c], Bartosz Setner[g], Łukasz Szczukowski[h], Zbigniew Szewczuk[g], Kazuto Yamauchi[d,f], Wiesław Malinka[h], Laurent Chavatte[a], Ryszard Łobinski[a,i]

[a]CNRS/UPPA, LCABIE, UMR5254, Hélioparc, 2, av. Pr. Angot, F-64053 Pau, France. Fax: 33-5594-07681; Tel: 33-5594-07739; E-mail: lukasz.szyrwiel@univ-pau.fr

[b]RIKEN SPring-8 Center, 1-1-1 Kouto, Sayo, Hyogo 679-5148, Japan

[c]Department of Intractable Diseases, Research institute, National Center for Global Health and Medicine, Tokyo 162-8655, Japan Fax: 81-3-32027364; Tel: 81-3-32027181; E-mail: mshimura@ri.ncgm.go.jp

[d]CREST, Japan Science and Technology Agency, Kawaguchi, Saitama 332-0012, Japan

[e]Inorganic Analysis Laboratories, Toray Research Center Inc., Otsu, Shiga 520-8567, Japan

[f]Department of Precision Science and Technology, Graduate School of Engineering, Osaka University, Suita, Osaka 565-0871, Japan

[g]Faculty of Chemistry, University of Wrocław, ul. F. Joliot-Curie 14, 50-383 Wrocław, Poland

[h]Department of Chemistry of Drugs, Wrocław Medical University, ul. Borowska 211, 50-552 Wrocław, Poland

[i]Chair of Analytical Chemistry, Warsaw University of Technology, ul. Noakowskiego 3, 00-664 Warszawa, Poland

* Corresponding author

Abstract

A TAT_{47-57} peptide was modified on the N-terminus by elongation with a 2,3-diaminopropionic acid residue and then by coupling of two histidine residues on its N-atoms. This branched peptide could bind Ni under physiological conditions as a 1:1 complex. We demonstrated that the complex was quantitatively taken up by human fibrosarcoma cells, in contrast to Ni^{2+} ions. Ni localization (especially at the nuclei) was confirmed by imaging using both scanning X-ray fluorescence microscopy and Newport Green fluorescence. A competitive assay with Newport Green showed that the latter displaced the peptide ligand from the Ni-complex. Ni^{2+} delivered as a complex with the designed peptide induced substantially more DNA damage than when introduced as a free ion. The availability of such a construct opens the way to investigate the importance of the nucleus as a target of the cytotoxicity, genotoxicity or carcinogenicity of Ni^{2+}.

Keywords: Tat peptide; Ni; branched peptide; X-ray fluorescence microscopy

Introduction

Cytotoxicity of Ni^{2+} ions is well-established[1] and referred to in terms of genotoxicity[2], carcinogenicity[3], and induction of oxidative stress.[4] The role of the cellular organelles such as nuclei, mitochondrion, and lysosomes in the toxicity remains unclear. Carcinogenetic activity is known to depend on the efficiency of Ni to enter the cell and reach chromatin.[3] In the nucleus, Ni is believed to bind with histone and inhibit histone acetylation, which suppresses gene expression.[1,3] The non-nuclear mechanisms include interactions with the iron regulatory protein-1[5] in hepatoma cells, putatively leading to a nickel-induced hypoxic response.[1] To increase our understanding of the mechanisms of toxicity of Ni^{2+} ions and the role of the various cell organelles, the development of Ni^{2+} ion transporter probes that selectively deliver Ni^{2+} to a target organelle and release it under appropriate conditions is required.

Cell-penetrating peptides, usually derived from viruses or mammalian proteins[6], have been increasingly applied in the transport (by chemical conjugation) of

drugs[7,8,9], genes[10,11] and nanoparticles[12,9] to specific cell organelles, such as the nucleus or mitochondrium.[13] In terms of specific delivery to the nucleus, the Trans-Activator of Transcription (TAT) protein of human immunodeficiency virus (HIV) is commonly used.[11,14] Specific delivery to the nucleus may be the result of an affinity between the lysine and arginine residues (which are positively charged under physiological pH and abundant in the TAT fragment) and the negatively charged DNA.[15]

The goal of this study was to explore the use of a TAT vector to deliver Ni^{2+} to the cell nucleus in a sufficiently labile complex to preserve its reactivity towards the molecules present in the nucleus. Limited information is available on the metal complexing properties of TAT_{47-57} (Fig. 1a). Indeed, a sequence rich in arginine and lysine does not have a high affinity to metals.[16,17] To our knowledge, the only attempt to use a TAT system for a similar purpose was based on the chemical conjugation of a quasi-covalent 99mTc[18,19] or Re and Cu[20,21] complexes, which was incompatible with our objective to preserve the metal reactivity in the nucleus required for inducing chemical toxicity.

The strategy developed in this report was based on elongation of the TAT_{47-57} (Fig 1a) sequence with a 2,3-diaminopropionic acid residue (Fig 1b). The fork created by the -HN-CH_2-CH(R)-NH- sequence allowed for further elongation of the peptide with a histidine residue via each of the nitrogen atoms (Fig 1c). The branching was expected to increase the proteolytic[22,23] stability and create an environment that allows for reversible binding of Ni^{2+}.

Experimental

Peptide synthesis.

All Fmoc amino acids, including Fmoc-L-Dap(Fmoc)-OH used as a branching amino acid, solvents, and reagents were purchased from Iris Biotech GmbH and used as received.

TAT_{47-57} synthesis. Synthesis of the TAT_{47-57} fragment (H-Tyr^{47}-Gly-Arg-Lys-Lys-Arg-Arg-Gln-Arg-Arg-Arg^{57}-OH) and TAT_{47-49} (H-Tyr^{47}-Gly^{48}-OH) was performed manually on the preloaded Wang resin (Fmoc-Arg(Pbf)-Wang resin, loading: 0.5 mM/g) in a polypropylene syringe reactor (Intavis, Köln, Germany) fitted with a

polyethylene filter, according to the standard Fmoc (9-fluorenylmethoxycarbonyl) solid-phase synthesis procedure. A total of 3 eq. of TBTU (*O*-(benzotriazol-1-yl)-*N*,*N*,*N*',*N*'-tetramethyluronium tetrafluoroborate) was used as a coupling reagent. A total of 3 eq. of Oxyma Pure (ethyl 2-cyano-2-(hydroxyimino)acetate) and 3 eq. of DIPEA (*N*,*N*-diisopropylethylamine) were used as additives. DMF (*N*,*N*-dimethylformamide) and fully protected peptide were washed with methanol and dried in a vacuum.

Dap branching. After removal of Fmoc protection from the N-terminal amino acid, Fmoc-Dap(Fmoc)-OH was coupled using a standard Fmoc solid-phase synthesis procedure (3 eq. of TBTU as a coupling reagent and 3 equiv. of each of the Oxyma Pure and DIPEA as an additive in DMF for 2 h). Completion of coupling was confirmed based on the Kaiser Test.

2 His peptide branch synthesis. Removal of both Fmoc protecting groups from Fmoc-Dap(Fmoc)-Tyr(^{t}Bu)^{47}-Gly-Arg(Pbf)-Lys(Boc)-Lys(Boc)-Arg(Pbf)-Arg(Pbf)-Gln(Trt)-Arg(Pbf)-Arg(Pbf)-Arg(Pbf)^{57}-Wang resin and Fmoc-Dap(Fmoc)-Tyr(^{t}Bu)-Gly-Rink Amide resin was achieved by repeated washing with 25% piperidine in DMF (3 and 17 min, respectively). A mixture of Fmoc-His(Boc)-OH/TBTU/Oxyma Pure/DIPEA (3 eq. of each reagent) in DMF for each unprotected amine group was added and stirred for 24 h. The completeness of the coupling reaction was confirmed using the Kaiser Test.

H-His-Dap(H-His)-TAT$_{47-57}$ and H-His-Dap(H-His)-TAT$_{47-48}$ cleavage from resin and purification. H-His-Dap(H-His)-TAT$_{47-57}$ and H-His-Dap(H-His)-TAT$_{47-48}$ were cleaved from the resin simultaneously with the side-chain deprotection using a solution of TFA/H_2O/TIS (95/2.5/2.5, v/v/v) at room temperature for 2 h. The peptide was purified using semi-preparative RP-HPLC on a Varian ProStar (Paolo Alto, CA) with UV detection (210 and 280 nm) on a TSKgel ODS-120T column (215 × 30 mm, 10 μm) equipped with a TSK guard column ODS (21.5 × 7.5 mm, 10 μm), with a gradient elution of 0−80% B in A (A: 0.1% TFA; B 0.1% TFA in 80% (v_A/v_B) acetonitrile) at 7 ml/min for 40 min. The purity of the obtained peptide was checked using analytical RP-HPLC on a Thermo Separation Product (Waltham, MA) on a YMC-Pack ODS-AQ12S05 column (250 × 4.6 mm, 5 μm) equipped with a guard cartridge system for HPLC using a gradient elution of 0−80% B in A (A: 0.1% TFA; B 0.1% TFA in 80% (v_A/v_B) acetonitrile) at 1 ml/min for 40 min. The H-His-

Dap(H-His)-TAT_{47-57} peptide was converted into the acetate form by repeated lyophilization from 1% acetic acid.[28] The molecular weight of peptides was confirmed using ESI-MS on a Bruker micrOTOF-Q mass spectrometer (Bruker Daltonik GmbH, Bremen, Germany). In the case of H-His-Dap(H-His)-TAT_{47-57}, $[M+4H^+]^{4+}$ was [found(calculated)] 480.7(480.8), $[M+5H^+]^{5+}$ 384.8(384.8), $[M+6H^+]^{6+}$ 320.8(320.8), $[M+7H^+]^{7+}$ 275.1(275.1), RT = 8.6. In case of H-His-Dap(H-His)-TAT_{47-57} $[M+H^+]^+$ 598.2(598.2), RT = 4.2.

Potentiometric measurements and UV-VIS spectroscopy

The peptide B protonation and the Ni^{2+} complex stability constants were calculated from three titration curves in the pH range 2.5 to 10.5 at 25°C under argon. Ligand concentration ranged from 1×10^{-3} to 1.5×10^{-3} M with a Ni^{2+}-to-ligand ratio of 0.95. The pH-metric titrations were performed in 0.1 M KCl using a Metrohm titrator fitted with a Mettler Toledo InLab®Micro combined electrode calibrated for $[H^+]$ with HCl. The complex stability constants and standard deviations were calculated using the HYPERQUAD 2013 software from three titrations for each investigated system.[23] Absorption spectra (300-900 nm) were recorded on PerkinElmer Lambda 25 spectrophotometer fitted with a 0.5-cm path quartz cell.

ESI-MS

The ESI-MS MS measurements were performed using Orbitrap Velos mass spectrometer (Thermo Fisher) in positive ion full scan (*m/z* 180–2000 Da) mode at 100,000 resolution. The apopeptide (A) was dissolved in 20 µM ammonium acetate buffer (pH 6.8) in 3% (v/v) methanol. Different quantities of nickel(II) acetate (Sigma-Aldrich) were added to cover the molar ratio range up to around 1 Ni : 1 A. Ligand concentration was constant in each measurement (6×10^{-5} M). For MS/MS experiments, the *m/z* 396.016 ion corresponding to the Ni-binding fragment was selected. The collision energy in the MS/MS experiments was 38 eV for HCD (Higher Energy Collision Dissociation). Data acquisition and treatment were performed using Xcalibur 2.1 (Thermo Fisher).

Cell treatment

Human fibrosarcoma cell line HT1080, which is commonly used to evaluate cytotoxicity due to pseudodiploids and tumor suppressor gene p53 activity[24,25,26],

]

was obtained from the Health Science Research Resources Bank (JCRB9113) of Japan (Tokyo, Japan). Cells were maintained in Dulbecco's modified Eagle's medium (DMEM, Nissui, Tokyo, Japan) supplemented with 10% heat-inactivated fetal calf serum (FBS, BioWhittaker, Walkersville, MD) and 2 mM glutamine (Wako, Osaka, Japan). Cells were plated 21 h prior to treatment. Culture medium was then replaced with pre-warmed 37°C CO_2 independent medium (#18045-088, GIBCO) containing 10% FBS. Ni-TAT, Ni^{2+}, or TAT was incubated for 0 to 30 min at 37°C. After treatment, cells were washed twice with PBS (-) (P-4417, Sigma) containing 10% FBS and then once with PBS (-). For ICP-MS analysis, cells were collected with a scraper (#3008, Coning, NY). Cells were centrifuged with 1000 × *g* at 5°C and counted.

Cell fractionation

For ICP-MS analysis, cells were collected with scraper (#3008, Coning, NY). Cells were centrifuged with × 1000g at 5 °C and counted, which was applied for whole cell analyses. To further obtain nuclear and cytoplasmic fractions, we use a combination of previously described methods.[26,27] Briefly, cells were re-suspended in Buffer N (15 mM Tris-HCl (pH 7.5), 60 mM KCl, 15 mM NaCl, 5 mM $MgCl_2$, 1 mM $CaCl_2$, 1 mM dithiothreitol, 2 mM sodium vanadate, 250 mM sucrose, protease inhibitor cocktail (Sigma-Aldrich), 1 mM phenylmethylsulfonyl fluoride (PMSF)). An equal volume of Buffer N containing 0.6% Nonidet P-40 was then added to the resuspended cells, and the resulting suspension was mixed gently and incubated on ice for 5 min. Nuclei were pelleted by centrifugation at 2,000 × g for 5 min at 4°C. Supernatant was additionally collected with three washes in Buffer N as a cytoplasmic fraction.

ICP-MS analysis

Cells were digested with 0.5 ml of HNO_3 at 180°C for 20 min using an ETHOS1 microwave oven (Milestone, Shelton, CT) and then made up with water to 5 mL. Concentrations of Ca and Mg were determined using ICP-AES (Optima 4300DV, PerkinElmer, Waltham, MA), and those of ^{55}Mn, ^{60}Ni and ^{63}Cu using ICP-SFMS (Element XR, Thermo Fisher Scientific, Bremen, Germany). These measurements were validated using standard human serum (Seronorm™ , Sero, Norway).

X-ray microscopy

Prolene film (JEOL, Tokyo, Japan) with carbon deposition (SC-701C-01, Sanyu Electron, Tokyo, Japan; JEE-420T, JEOL) based on acrylic plates were prepared for cellular basement, which was submerged in 70% EtOH for spectroscopic analysis (Wako Pure Chemical, Osaka Japan) for 10 min and again with fresh 70% EtOH at least for 8 h for sterilization. A plate was then washed twice with DMEM without FBS. Cells were plated 21 h prior to treatment, as described above. Culture medium was replaced with 37°C CO_2-independent medium containing 10% FBS prior to the treatment. After the treatment, cells were washed with PBS (-) containing 10% FBS twice, and washed once with PBS (-). Cells were fixed with 2% PFA (#18814, ultra pure EM grade, Polysciences Inc., PA) in PBS (-) for 10 min. Plates were washed with PBS (-) once and 70% EtOH twice, air dried, and stored in a clean culture dish. Scanning X-ray fluorescence microscopy (SXFM) was performed using the undulator beamline, BL29XU, of the SPring-8 synchrotron radiation facility by combining a Kirkpatrick-Baez type X-ray focusing system, an xy-scanning stage for sample mounting, and an energy dispersive X-ray detector (Vortex-90EX, Hitachi High-Technologies Science America Lovation).[27,28] Monochromatic X-rays at 15 keV and a flux of ~2×10^{11} photon/s were focused on a 1000 × 1000-nm spot. The X-ray fluorescence spectrum was recorded with an exposure of 1 s at each pixel. The fluorescence signals of each element of interest were extracted and normalized based on incident beam intensity. After scanning the whole area, elemental distributions were digitally visualized. In addition to the mapping images, an elemental concentration per μm^2 was quantitatively analyzed using thin Ni films, of which the thickness and the density were decided in advance.[28]

Newport Green fluorescence

Cells were plated in a glassbase dish (Mastunami Glass) and pretreated with 5 μM Newport Green (Invitrogen, Paisley, UK) with DMEM containing 10% FBS for 30 min at 37°C, and washed once with CO_2-independent medium (#18045-088, GIBCO) containing 10% FBS. Immediately after pretreatment, cells were placed on a thermo plate (IX-HP100; Olympus) to maintain growth at 37°C. Fluorescence signals (excitation at 488 nm and emission at 530 nm) and DIC images were taken with a fluorescence microscope (IX70; Olympus). Photographs were taken using a charge-coupled device camera (Sensys 1400; Photometrics) for analysis. Signal intensities per unit area in TIFF images acquired using IPLab. The signal intensity

was measured using the ImageJ software.

Immunofluorescence microscopy.

Immunofluorescence staining was performed as described previously.[24,25,26] Briefly, the cells were washed in PBS, fixed in 2% paraformaldehyde in PBS for 10 min, permeabilized with 0.2% Triton X-100 in PBS for 10 min, and blocked with 10% goat serum in PBS. Primary antibody against phospho-histone H2A.X (ser139)[29], clone JBW301 (1:5000, Millipore, Billerica, MA), was applied. Then, the slides were incubated with goat anti-mouse IgG secondary antibody, Cy3 conjugate (1:1000; Invitrogen, Oslo, Norway). The slides were stained with Hoechst 33342 to visualize DNA, mounted in anti-fade mounting medium (Kirkegaard & Perry Laboratories, Gaithersburg, MD), and observed under an Olympus BX50 microscope (Olympus, Melville, NY) equipped with a Plan Apochromat objective lens with immersion oil (nd=1.516 at 23°C, Olympus) and a SenSys CCD camera (Photometrics, Tucson, AZ). Images were acquired using IPLab Spectrum software (Scanalytics, Billerica, MA). The TIFF images acquired using IPLab Spectrum were imported into Photoshop (Adobe). The signal intensities per unit area and cellular area in the TIFF images over 100 cells were acquired using Image J software (National Institutes of Health, Bethesda, MD).

Statistical analysis

Statistical analyses were performed using a two-tailed unpaired t test. P-values < 0.05 were considered statistically significant.

Results and Discussion

Ni^{2+} forms a 1:1 complex with the synthesized TAT-based branched peptide

Electrospray ionization MS revealed an isotopic envelope at m/z 396 upon the addition of Ni to the solution of synthesized peptide (A) (Fig. 2). This signal corresponded to a quintuple charged ion with the molecular formula $Ni(C_{79}H_{141}N_{40}O_{17})$, which is in agreement with the formation of a 1:1 Ni^{2+}-A complex. The appearance of this peak is accompanied by the disappearance of a peak at m/z 385, corresponding to the quintuple charged ion of the apopeptide. The presence of both peaks in the mass spectrum of a 1:1 Ni-A complex is indicative of a fairly labile complexation. The fragmentation HCD (Higher Energy Collision

Dissociation) of the parent ion gives a peak at m/z 195 (Fig. 3), corresponding to the molecular formula $Ni(C_{14}H_{20}N_8O_2)$, which is in agreement with the hypothesis of one Ni^{2+} ion entering the branch (Fig. 1c) of the synthesized peptide.

The Ni^{2+} - branch peptide complex (NiA) is stable under physiological conditions

To avoid interference of deprotonation on the high number of Lys and Arg residues in the new branched peptide (A) (Fig. S1), a structural analog of the branched-TAT peptide H-His-Dap(H-His)-Tyr-Gly-NH_2 (B) was synthesized (Fig. S1) to measure Ni^{2+} complexation efficiency. The stability constants indicate that under physiological conditions, Ni^{2+} is quantitatively present as the NiHB complex, and the pNi^{2+} ($-\log[Ni^{2+}]$) at pH 7.4 is 5.9. The coordination properties of (B) over the entire pH range are discussed in Fig. S2.

Cells uptake NiA complex, but not Ni^{2+}

Fig. 4 shows that the uptake (measured by ICP-MS and ICP-AES) of elements typically present in cell culture medium (Ca, Mg, Cu, Mn, Zn). These elements are not affected by the addition of Ni^{2+} (Fig. 4, Ni^{2+}), free peptide (Fig. 4, A), or the Ni-peptide complex (Fig. 4, NiA). In addition, Ni^{2+} is not taken up from the culture medium (Fig. 4, Med.). However, when Ni^{2+} is supplied as the Ni-A complex, it is efficiently taken up after 20 min (Fig. 4, NiA). This observation is supported by the results of the fluorescence measurements using Newport Green™ (NPG) in Figs. 5 and S3 where nickel uptake in cells was shown. Note that NPG is not selective to Ni and responds to the presence of other ions, such as Zn^{2+}, hence the need to confirm the presence of Ni using SXFM and ICP-MS.

NiA complex is transported to the nuclei

The determination of Ni in the nuclei pellet and cytosol separated by centrifugation indicates that over 80% of Ni in cells was found in the nuclear fraction based on ICP-MS (Fig. S4). The nuclear location of Ni was further confirmed using X-ray fluorescence imaging (SXFM) (Figs. 6 and S5). Using SXFM, nuclear localization was not observed in all of the cells examined and Ni-signals were also present at the membrane (SFig. 4). However, we did not observe an NPG fluorescence signal only at the membrane using living cells (Fig. 7). This might be due to the fact that we prepared cells with fixation and EtOH washing for SXFM, which might remove

soluble Ni-complexes. The Ni signals from SXFM are thought to be from insoluble Ni-complex associated with chromatin or membranes. In addition, SXFM data confirm the high Ni uptake when supplied as NiA, but not as Ni^{2+}. The nuclear localization of Ni was further corroborated based on NPG fluorescence in living cells (Fig. 7). The use of the NPG probe suffers from the risk of contamination by other elements, especially Zn. However, the difference at 20 min is clearly assigned to the NiA that penetrated the cell. These data support the Ni^{2+} nuclear transporting properties of the new branched peptide complex (NiA). The NPG fluorescence in the nuclear region (Fig. 7) confirms the ESI MS (Fig. 2) and potentiometric titration data (Fig. S2), and suggests that the Ni-TAT complex is sufficiently labile to allow the TAT ligand to exchange with NPG, which makes it a transporter of reactive Ni.

NiA complex induced DNA damage, but not Ni^{2+}

Based on these results, we evaluated the DNA damage induced by NiA. NiA (50 μM) induced significant formation of γ-H2AX foci, a marker of DNA double-strand breaks,[29] whereas 50 μM Ni ions did not cause any changes (Figs. 8a, 8b). Interestingly, the γ-H2AX signals from 50 μM NiA-treated cells ranged widely. Some cells showed even stronger signals than cells treated with 500 μM Ni ions (Fig. 8c). The larger nuclear size with NiA compared with 50 μM Ni ions was suggestive of growth inhibition (Figs. 8b, 8c). These data suggest that NiA is an active Ni ion nuclear transporter that induces DNA damage.

Conclusions

The design of the branched TAT peptide allowed for the development of a novel type of Ni^{2+} transporter that can carry Ni^{2+} ion into nuclei of human cells. The stability of the complex (pNi^{2+} 5.9) was sufficiently low to allow ligand exchange with NPG, and thus (potentially) with other chemical molecules present in the nucleus. The study offers a tool for the delineation of specific mechanisms of Ni cellular toxicity. Replacement of the histidine in the final step of the synthesis by other ligands may produce probes with different reactivities in the nuclei and facilitate application of this tool to other metals. The availability of such a construct opens the way to investigate the importance of the nucleus as a target of the cytotoxicity, genotoxicity or carcinogenicity of Ni^{2+}, comparing with the toxicity upon simple exposure to Ni^{2+}.

Disclosure

The authors report no conflicts of interest.

Author contributions

L.Sz., M.S., R.L planned the experiments; L.Sz., M.S., S.M., K.Y., B.S., A.M., Z.Sz., L.Sz., W.M., J.S. performed the experiments and analysed the data; L.Sz., M.S. R.L., L.C. wrote manuscript. All authors have discussed the results of the manuscript.

Acknowledgments

We thank Dr. Yoshiki Komura at Riken Institute for their assistance with X-ray microscopy, and Dr. Yutaka Iida at Toray Research Center, Inc. and Prof. Tetsuya Ishikawa at Riken for careful advice and encouragement during this study. This study was supported by a Polish Foundation of Science within the POMOST program co-financed by the European Union within European Regional Development Fund (POMOST/2012-5/9) and Grant-in-Aid and Research on Advanced Medical Technology, Ministry of Health, Labor, and Welfare of Japan, CREST from the Japan Science and Technology Agency. Lukasz Szyrwiel was supported by a Marie Curie Intra European Fellowship from the European Union (PIEF-GA-2012-329969).

Additional Information

Supplementary Information accompanies this paper

Bibliography

1. K. Salnikow and K. S. Kasprzak, in *Nickel and Its Surprising Impact in Nature*, John Wiley & Sons, Ltd, 2007, pp. 581–618.

2. K.S. Cameron, V. Buchner and P.B. Tchounwou, *Reviews on environmental health*, 2011, **28**, 81–82.

3. M. Costa and C. B. Klein, *Enviromental Health Perspectives*, 1999, **107**, 438–439.

4. K. Das and V. Buchner, *Reviews on Environmental Health*, 2007, 22, 157–173.

5. S. Oshiro, K. Nozawa, M. Hori, C. Zhang, Y. Hashimoto, S. Kitajima, and K. Kawamura, *Biochemical and Biophysical Research Communications*, 2002, **290**, 213–218.

6. F. Milletti, *Drug Discovery Today*, 2012, **17**, 850–860.

7. H. Sakhrani, NM. Padh, *Drug Design, Development and Therapy*, 2013, **7**, 585—599.

8. S. El-andaloussi, P. Järver, H. J. Johansson, and Ü. Langel, *Biochemical Journal*, 2007, **407**, 285–292.

9. L. Pan, Q. He, J. Liu, Y. Chen, M. Ma, L. Zhang, and J. Shi, *Journal of the American Chemical Society*, 2012, **134**, 5722–5725.

10. K. Welser, F. Campbell, L. Kudsiova, A. Mohammadi, N. Dawson, S. L. Hart, D. J. Barlow, H. C. Hailes, M. J. Lawrence, and A. B. Tabor, *Molecular pharmaceutics*, 2013, **10**, 127–41.

11. Y. Liu, Y. J. Kim, M. Ji, J. Fang, N. Siriwon, L. I. Zhang, and P. Wang, *Molecular Therapy — Methods & Clinical Development*, 2014, **1**.

12. C. C. Berry, *Nanomedicine*, 2008, **3**, 357–365.

13. K. L. Horton, K. M. Stewart, S. B. Fonseca, Q. Guo, and S. O. Kelley, *Chemistry & Biology*, 2008, **15**, 375–382.

14. H. Brooks, B. Lebleu, and E. Vivès, *Advanced Drug Delivery Reviews*, 2005, **57**, 559–577.

15. A. Subrizi, E. Tuominen, A. Bunker, T. Róg, M. Antopolsky, and A. Urtti, *Journal of Controlled Release*, 2012, **158**, 277–285.

16. H. Kozłowski, W. Bal, M. Dyba, and T. Kowalik-Jankowska, *Coordination Chemistry Reviews*, 1999, **184**, 319–346.

17. I. Sóvágó, C. Kállay, and K. Várnagy, *Coordination Chemistry Reviews*, 2012, **256**, 2225–2233.

18. K. E. Bullok, M. Dyszlewski, J. L. Prior, C. M. Pica, V. Sharma, and D. Piwnica-Worms, *Bioconjugate Chemistry*, 2002, **13**, 1226–1237.

19. V. Polyakov, V. Sharma, J. L. Dahlheimer, C. M. Pica, G. D. Luker, and D. Piwnica-Worms, *Bioconjugate Chemistry*, 2000, **11**, 762–771.

20. Y. Kanemaru, Y. Momiki, S. Matsuura, T. Horikawa, J. Gohda, J. Inoue, Y. Okamoto, M. Fujita, and M. Otsuka, *Chemical and Pharmaceutical Bulletin*, 2011, **59**, 1555–1558.

21. A. Leonidova, V. Pierroz, L. A. Adams, N. Barlow, S. Ferrari, B. Graham, and G. Gasser, *ACS Medicinal Chemistry Letters*, 2014, **5**, 809–814.

22. L. Bracci, C. Falciani, B. Lelli, L. Lozzi, Y. Runci, A. Pini, M. G. De Montis, A. Tagliamonte, and P. Neri, *Journal of Biological Chemistry* , 2003, **278** , 46590–46595.

23. P. Gans, A. Sabatini, and A. Vacca, *Talanta*, 1996, **43**, 1739–1753.

24. M. Shimura, Y. Tanaka, S. Nakamura, Y. Minemoto, K. Yamashita, K. Hatake, F. Takaku, and Y. Ishizaka, *The FASEB Journal*, 1999, **13**, 621–637.

25. H. Tachiwana, M. Shimura, C. Nakai-Murakami, K. Tokunaga, Y. Takizawa, T. Sata, H. Kurumizaka, and Y. Ishizaka, *Cancer Research*, 2006, **66**, 627–631.

26. M. Shimura, Y. Toyoda, K. Iijima, M. Kinomoto, K. Tokunaga, K. Yoda, M. Yanagida, T. Sata, and Y. Ishizaka, *The Journal of Cell Biology*, 2011, **194**, 721–735.

27. M. Shimura, A. Saito, S. Matsuyama, T. Sakuma, Y. Terui, K. Ueno, H. Yumoto, K. Yamauchi, K. Yamamura, H. Mimura, Y. Sano, M. Yabashi, K. Tamasaku, K. Nishio, Y. Nishino, K. Endo, K. Hatake, Y. Mori, Y. Ishizaka, and T. Ishikawa, *Cancer Research*, 2005, **65**, 4998–5002.

28. S. Matsuyama, M. Shimura, H. Mimura, M. Fujii, H. Yumoto, Y. Sano, M. Yabashi, Y. Nishino, K. Tamasaku, T. Ishikawa, and K. Yamauchi, *X-Ray Spectrometry*, 2009, **38**, 89–94.

29. E. P. Rogakou, D. R. Pilch, A. H. Orr, V. S. Ivanova, and W. M. Bonner, *Journal of Biological Chemistry* , 1998, **273** , 5858–5868.

30. K. S. Bai and A. E. Martell, *Journal of the American Chemical Society*, 1969, **91**, 4412–4420.

Figure captions

Figure 1. The scheme of a) TAT_{47-57}, b) Dap-TAT_{47-57}, and c) H-His-Dap(H-His)-TAT_{47-57}, which is named A.

Figure 2. (+)ESI-MS mass spectra for the systems containing Ni and A at the following ratios: a) 0 Ni: 1 A, b) 0.6 Ni: 1 A, c) 1 Ni: 1 A ($C_A = 6 \times 10^{-5}$ M), d) fragment of experimental spectra corresponding to simulated signal of protonated peptide A $(C_{79}H_{143}N_{40}O_{17})^{5+}$, and e) fragment of experimental spectra corresponding to simulated signal of complex NiA - $Ni(C_{79}H_{141}N_{40}O_{17})^{5+}$.

Figure 3. HCD MS/MS spectra of the NiA showing the signal corresponding to the structural formula of possible isomers with *m/z* = 195.05 $(Ni(C_{14}H_{20}N_8O_2)^{2+}$).

Figure 4. Contents of selected elements in cells incubated with: Med., culture medium; Ni2+, Ni ions; NiA and A in function of time: 1, 10 min; 2, 20 min; 3, 30 min (Ca and Mg were determined by ICP-AES and Mn, Ni, Cu and Zn by ICP-MS).

Figure 5. Representative NPG images after treatment with Ni ion and NiA in living cells. NPG signal peaked at 20 min after NiA addition. Green, differential interference contrast (DIC) images; Red, NPG fluorescence. Bar, 20 μm. NPG fluorescence intensity was measured using cells (>50) at each time point. Values

represent the means ± SD of triplicates. Similar results were obtained in three independent experiments.

Figure 6. X-ray fluorescence images. From left, signals of P, Ni, and DIC images are shown. Each set of panels, cells treated with 20 μM of Ni ion (top) and NiA (bottom) for 20 min. P, phosphorus; Ni, nickel; DIC, differential interference contrast images. Brighter color indicates a higher signal intensity. Color bar, fg/μm^2; Bar, 10 μm.

Figure 7. Representative NPG images after treatment with Ni ion and NiA in living cells. Green, differential interference contrast (DIC) images; Red, NPG fluorescence. Bar, 10 μm.

Figure 8. γ-H2AX foci formation in NiA-treated cells. a) Representative images of γ-H2AX immunostaining. Green, DNA; red, γ-H2AX; Bar, 10 μm. b) Quantification of the γ-H2AX signal intensity at nuclei and nuclear size from cells (>100). Note that the signal in the 50 μM NiA-treated cells was significantly higher than in the 50 μM Ni ion-treated cells. Points show the values for each cell. The horizontal bar represents the mean. *** P<0.0001. c) The γ-H2AX signal intensity and nuclear size were plotted (>100). Cont, control; Ni 50: 50 μM nickel ion-treated cells at 48 h; NiA 50: 50 μM NiA-treated cells at 48 h; Ni 500: 500 μM nickel ion-treated cells at 48 h. Similar results were obtained in independent experiments.

Supplementary figure captions

Figure S1. Schematic structures of branch peptides: a) H-His-Dap(H-His)-Tyr-Gly-Arg-Lys-Lys-Arg-Arg-Gln-Arg-Arg-Arg-OH (A), b) H-His-Dap(H-His)-Tyr-Gly-NH_2 (B).

Figure S2. Speciation diagram for the system containing Ni^{2+} and B peptide, [Ni^{2+}] = 1×10^{-3} M, 1:1 M: B ratio (a). The physiological pH range is indicated by red dots. The logarithms of the protonation constants ($\log\beta_{HxL}$) and metal complex stability constants ($\log\beta_{NiHxL}$) for Ni^{2+} species with B, UV-Vis data for observed species (b).

The data showed that increases in pH from 4 to 5 resulted in the formation of minor NiH_2B species, which coexisted in equilibrium with the NiHB form. Unfortunately, the low concentration did not allow for precise determination of spectroscopic parameters for NiH_2B species. Near pH 5, the NiHB form started to be predominant up to pH 8. The involvement of peptide amide (N^-) donors in metal coordination was

observed when pH increased to 9. Then, two simultaneous deprotonations were observed, and complex $NiH_{-1}B$ was formed. The double deprotonation was also observed in cases of N,N'-diglycylethylenediamine (DGEN) ligand[30], which is an analog of the Ni-binding domain in the B ligand. Formation of the $NiH_{-1}B$ square planar complex with the $\{2NH_2, 2N^-\}$ donor set was also confirmed based on UV-Vis spectroscopy parameters, which clearly corresponded to those observed in similar Ni^{2+} complexes with the DGEN ligand ($\lambda = 414$, $\varepsilon = 219$).[30] Further increases in the pH resulted in deprotonation of non-coordinated tyrosine residue. However, changes of pK = 0.4 logarithmic units were suggestive of minor interactions.

Figure S3. Representative NPG images after treatment with Ni ion and NiA in living cells. Left, DIC image; right, NPG images. It was notable that the NPG signal intensity peaked 20 min after NiA addition. Bar, 50 μm.

Figure S4. Measured by ICP-MS amount of Ni in cytoplasmic and nuclear fraction of cells incubated in Ni free medium with Ni ions and NiA complex. Cyto, soluble cytoplasmic fraction; Nuc, whole nuclear and insoluble membrane fraction; Med, culture medium.

Figure S5. X-ray fluorescence images. From the left, signals of P, Zn, Ni, and DIC images are shown. Each set of panel, control cells (top), and cells treated with 20 μM of Ni ion (middle) and NiA for 20 min (bottom). P, phosphorus; Zn, zinc; Ni, nickel; P-Ni, merged images between phosphorus and nickel; DIC, differential interference contrast images. Brighter colour indicates higher signal intensity. Colour bar, $fg/\mu m^2$; Bar, 10 μm.

]

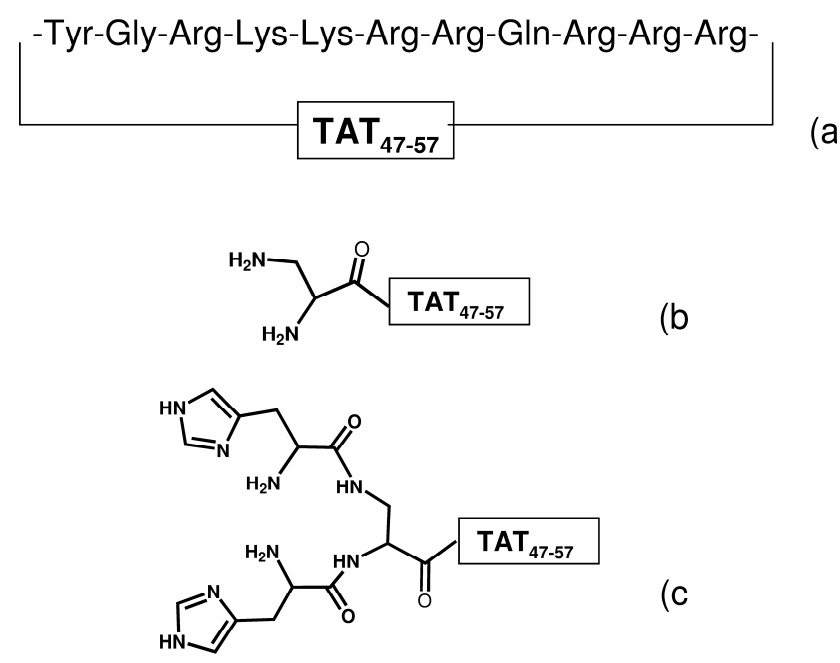

Figure 1. The scheme of a) TAT_{47-57}, b) Dap-TAT_{47-57}, and c) H-His-Dap(H-His)-TAT_{47-57}, which is named A.

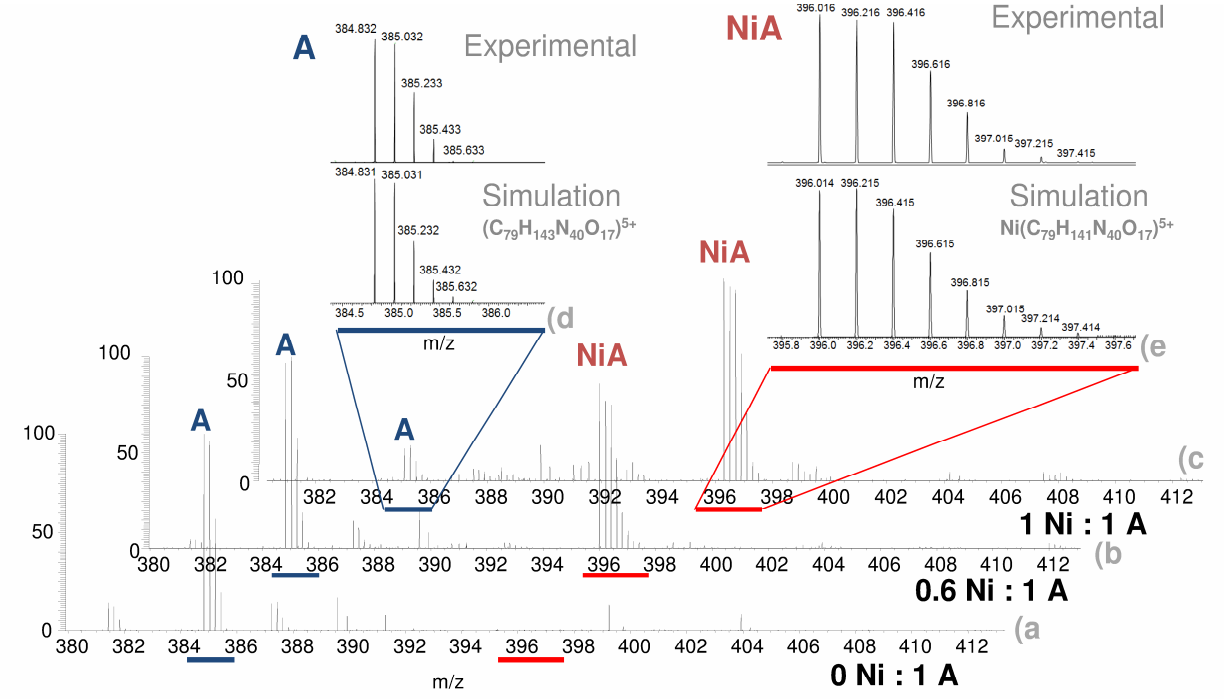

Figure 2. (+)ESI-MS mass spectra for the systems containing Ni and A at the following ratios: a) 0 Ni: 1 A, b) 0.6 Ni: 1 A, c) 1 Ni: 1 A (C_A= 6 × 10^{-5} M), d) fragment of experimental spectra corresponding to simulated signal of protonated peptide A $(C_{79}H_{143}N_{40}O_{17})^{5+}$, and e) fragment of experimental spectra corresponding to simulated signal of complex NiA - $Ni(C_{79}H_{141}N_{40}O_{17})^{5+}$.

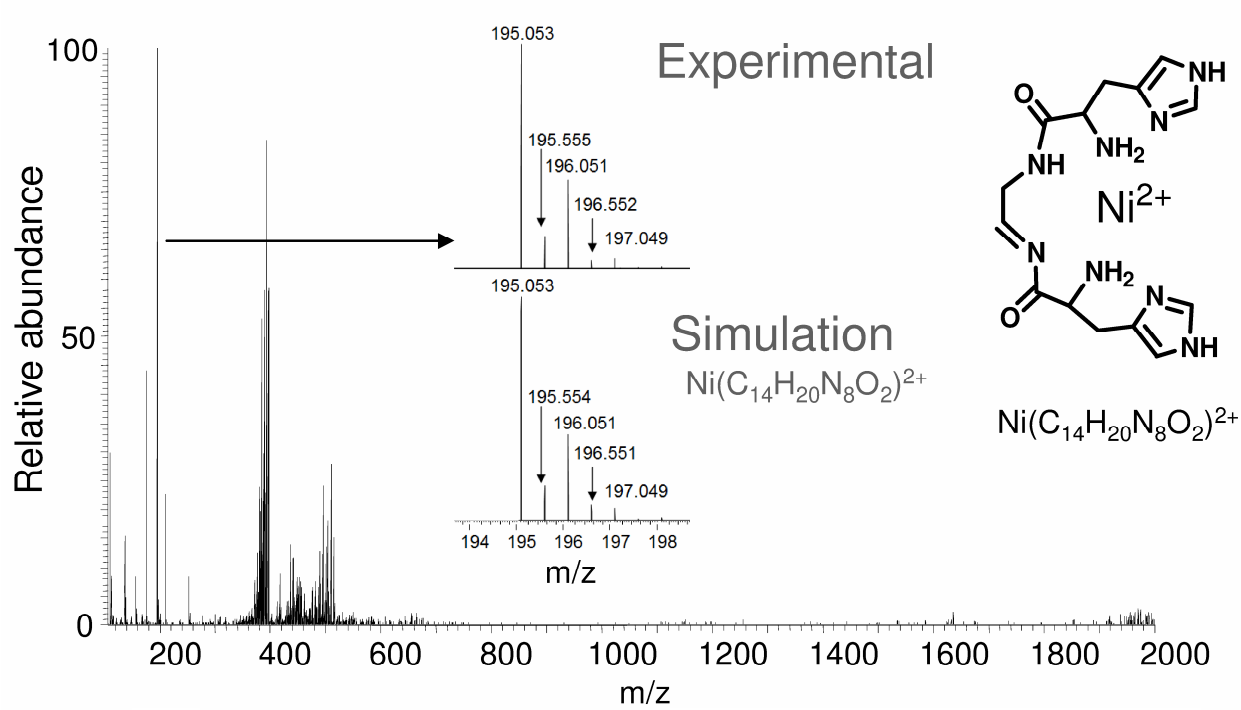

Figure 3. HCD MS/MS spectra of the NiA showing the signal corresponding to the structural formula of possible isomers with *m/z* = 195.05 ($Ni(C_{14}H_{20}N_8O_2)^{2+}$).

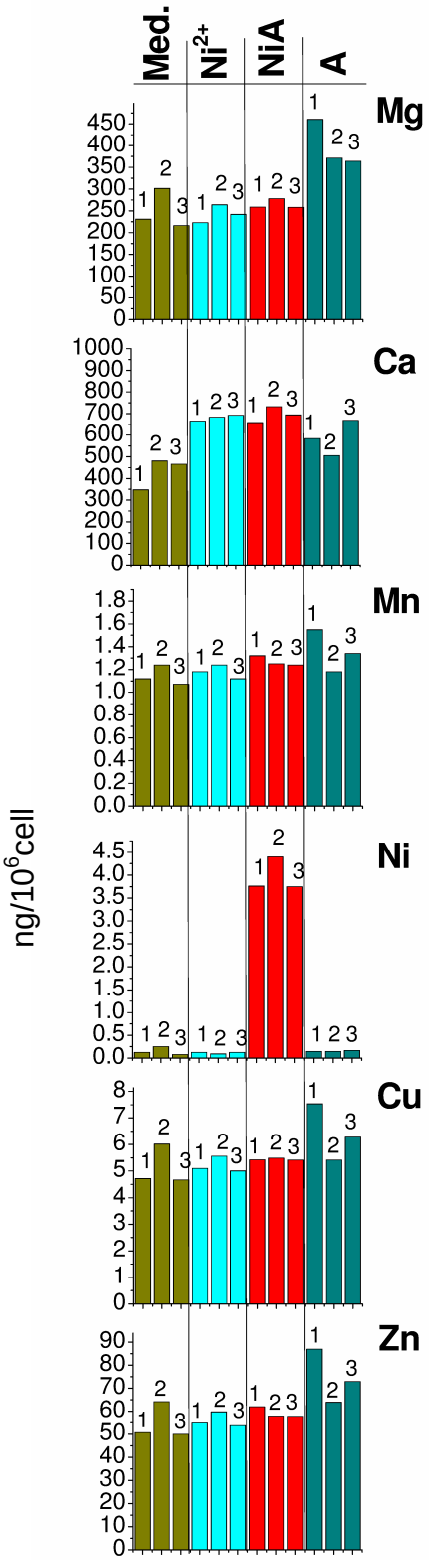

Figure 4. Contents of selected elements in cells incubated with: Med., culture medium; Ni^{2+}, Ni ions; NiA and A in function of time: 1, 10 min; 2, 20 min; 3, 30 min (Ca and Mg were determined by ICP-AES and Mn, Ni, Cu and Zn by ICP-MS).

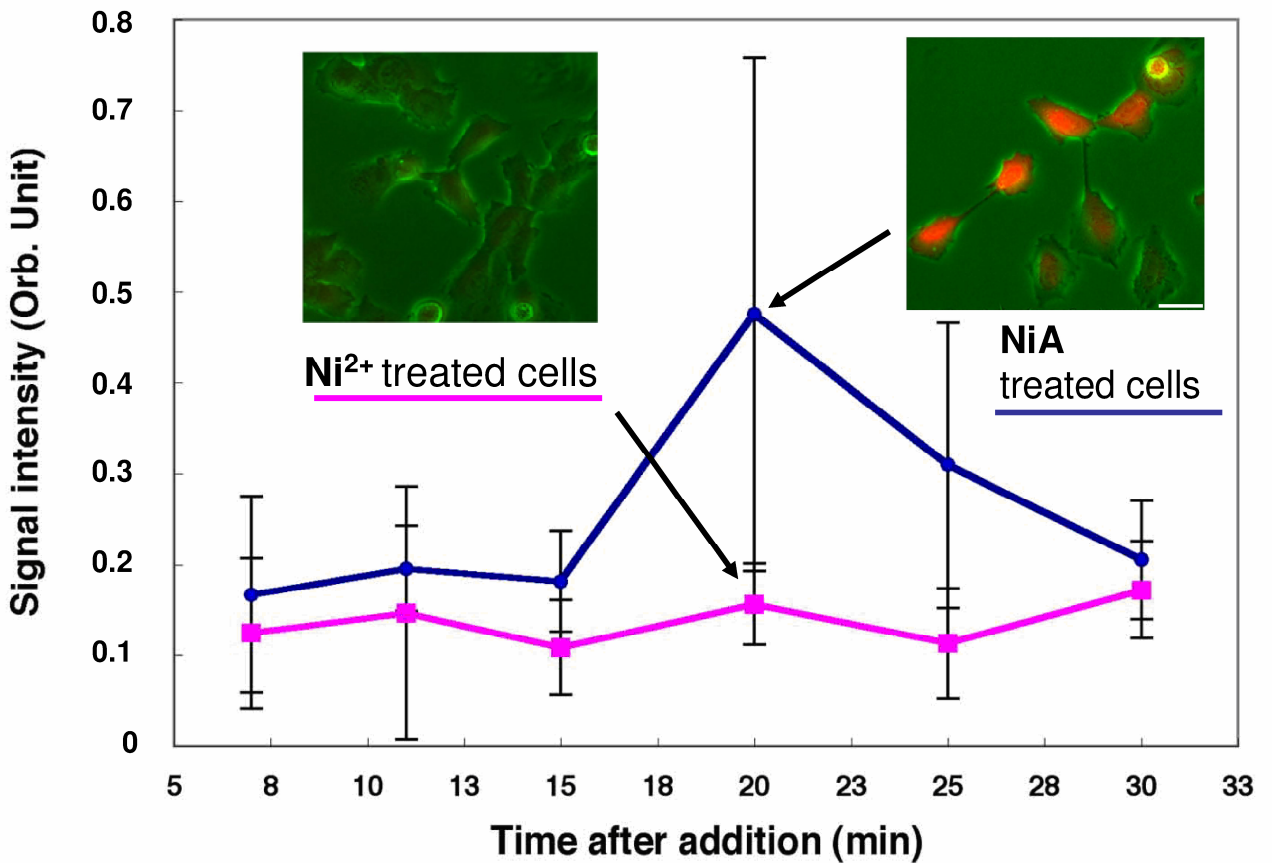

Figure 5. Representative NPG images after treatment with Ni ion and NiA in living cells. NPG signal peaked at 20 min after NiA addition. Green, differential interference contrast (DIC) images; Red, NPG fluorescence. Bar, 20 μm. NPG fluorescence intensity was measured using cells (>50) at each time point. Values represent the means ± SD of triplicates. Similar results were obtained in three independent experiments.

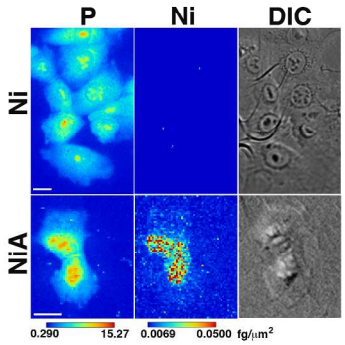

Figure 6. X-ray fluorescence images. From left, signals of P, Ni, and DIC images are shown. Each set of panels, cells treated with 20 μM of Ni ion (top) and NiA (bottom) for 20 min. P, phosphorus; Ni, nickel; DIC, differential interference contrast images. Brighter color indicates a higher signal intensity. Color bar, fg/μm2; Bar, 10 μm.

209x297mm (300 x 300 DPI)

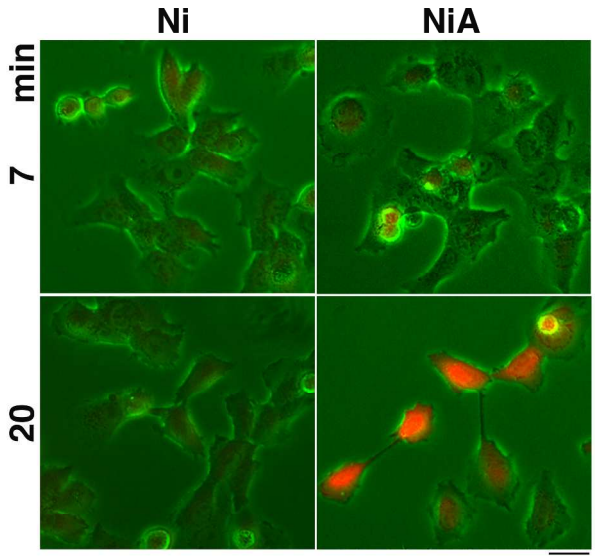

Figure 7. Representative NPG images after treatment with Ni ion and NiA in living cells. Green, differential interference contrast (DIC) images; Red, NPG fluorescence. Bar, 10 µm.

209x297mm (300 x 300 DPI)

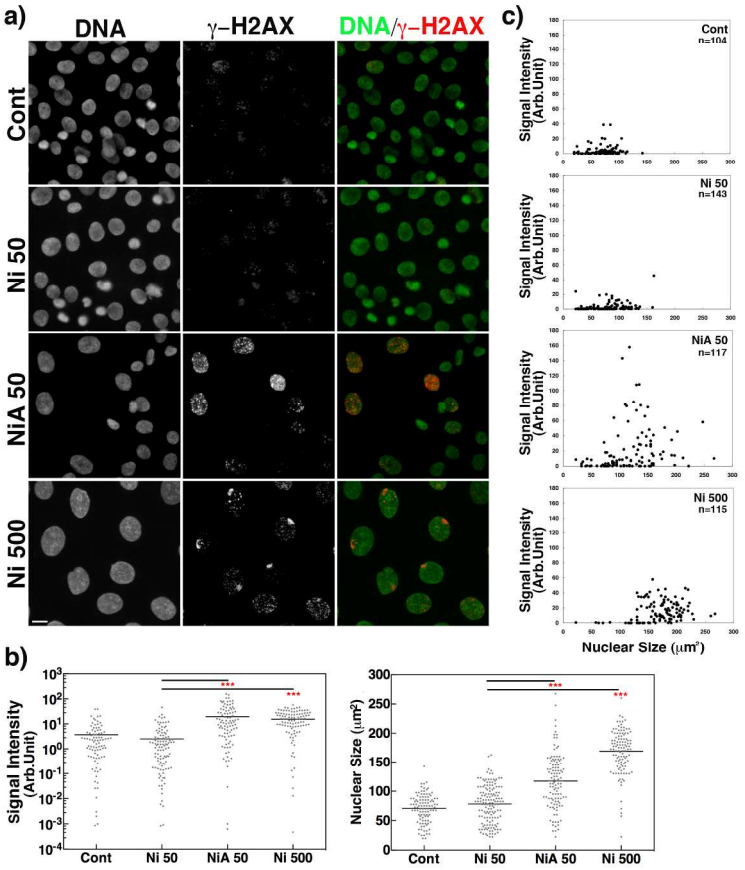

Figure 8. γ-H2AX foci formation in NiA-treated cells. a) Representative images of γ-H2AX immunostaining. Green, DNA; red, γ-H2AX; Bar, 10 μm. b) Quantification of the γ-H2AX signal intensity at nuclei and nuclear size from cells (>100). Note that he signal in the 50 μM NiA-treated cells was significantly higher than in the 50 μM Ni ion-treated cells. Points show the values for each cell. The horizontal bar represents the mean. *** P<0.0001. c) The γ-H2AX signal intensity and nuclear size were plotted (>100). Cont, control; Ni 50: 50 μM nickel ion-treated cells at 48 h; NiA 50: 50 μM NiA-treated cells at 48 h; Ni 500: 500 μM nickel ion-treated cells at 48 h. Similar results were obtained in independent experiments.

209x297mm (300 x 300 DPI)